Progress in Photovoltaics: Research and Applications

WILEY

PROGRESS IN PHOTOVOLTAICS

SHORT COMMUNICATION

Solar Cell Efficiency Tables (Version 65)

Martin A. Green[1] | Ewan D. Dunlop[2] | Masahiro Yoshita[3] | Nikos Kopidakis[4] | Karsten Bothe[5] | Gerald Siefer[6] | Xiaojing Hao[1] | Jessica Yajie Jiang[1]

[1]Australian Centre for Advanced Photovoltaics, School of Photovoltaic and Renewable Energy Engineering, University of New South Wales, Sydney, Australia | [2]European Commission–Joint Research Centre, Ispra, Varese, Italy | [3]Renewable Energy Research Center (RENRC), National Institute of Advanced Industrial Science and Technology (AIST), Tsukuba, Ibaraki, Japan | [4]National Renewable Energy Laboratory, Golden, Colorado, USA | [5]Calibration and Test Center (CalTeC), Solar Cells Laboratory, Institut für Solarenergieforschung GmbH (ISFH), Emmerthal, Germany | [6]Fraunhofer-Institute for Solar Energy Systems–ISE CalLab, Freiburg, Germany

Correspondence: Martin A. Green (m.green@unsw.edu.au)

Received: 26 September 2024 | **Revised:** 16 October 2024 | **Accepted:** 21 October 2024

Funding: This study was supported by the Australian Renewable Energy Agency, Grant/Award Number: SRI-001; U.S. Department of Energy (Office of Science, Office of Basic Energy Sciences and Energy Efficiency and Renewable Energy, Solar Energy Technology Program), Grant/Award Number: DE-AC36-08-GO28308; and Ministry of Economy, Trade and Industry.

Keywords: energy conversion efficiency | photovoltaic efficiency | solar cell efficiency

ABSTRACT

Consolidated tables showing an extensive listing of the highest independently confirmed efficiencies for solar cells and modules are presented. Guidelines for inclusion of results into these tables are outlined, and new entries since July 2024 are reviewed.

1 | Introduction

Since January 1993, '*Progress in Photovoltaics*' has published six monthly listings of the highest confirmed efficiencies for a range of photovoltaic cell and module technologies [1–3]. Providing guidelines for the inclusion of results into these tables not only provides an authoritative summary of the current state of the art but also encourages researchers to seek independent confirmation of results and to report results on a standardized basis. In Version 33 of these tables, results were updated to the new internationally accepted reference spectrum (International Electrotechnical Commission IEC 60904-3, Ed. 2, 2008).

The most important criterion for the inclusion of results into the tables is that they must have been independently measured by a recognized test centre listed in Versions 61 and 62 (also updated in 64). A distinction is made between three different eligible definitions of cell area: total area, aperture area and designated illumination area, as also defined elsewhere [2] (note that, if masking is used, masks must have a simple aperture geometry, such as square, rectangular or circular—masks with multiple openings are not eligible). 'Active area' efficiencies are not included. There are also certain minimum values of the area sought for the different device types (above 0.05 cm^2 for a concentrator cell, 1 cm^2 for a one-sun cell, 200 cm^2 for a 'submodule' and 800 cm^2 for a module).

Tabled results are reported for cells and modules made from different semiconductors and for subcategories within each semiconductor grouping. From Version 36 onwards, spectral response information is included (when possible) in the form of a plot of the external quantum efficiency (EQE) versus wavelength, either as absolute values or normalized to the peak measured value. Current–voltage (IV) curves have also been included where possible from Version 38 onwards.

The highest confirmed 'one sun' cell and module results are reported in Tables 1, 2, 3 and 4. Any changes in the tables from those previously published [1] **are set in bold type**. In most cases, a literature reference is provided that describes either the result reported, or a similar result (readers identifying improved references are welcome to submit to the lead author). Table 1 summarizes the best-reported measurements for 'one-sun' (non-concentrator) single-junction cells and submodules.

TABLE 1 | Confirmed single-junction terrestrial cell and submodule efficiencies measured under the global AM1.5 spectrum (1000 W/m²) at 25°C (IEC 60904-3: 2008 or ASTM G-173-03 global).

Classification	Efficiency (%)	Area (cm²)	V_{oc} (V)	J_{sc} (mA/cm²)	Fill factor (%)	Test centre (date)	Description
Silicon							
Si (crystalline cell)	**27.4 ± 0.4[a]**	**165.72 (t)**	**0.7456**	**42.35[b]**	**86.7**	**ISFH (9/24)**	**LONGi, n-type HTBC** [4]
Si (thin transfer submodule)	21.2 ± 0.4	239.7 (ap)	0.687[c]	38.50[c,d]	80.3	NREL (4/14)	Solexel (35 µm thick) [5]
Si (thin-film minimodule)	10.5 ± 0.3	94.0 (ap)	0.492[c]	29.7[c,e]	72.1	FhG-ISE (8/07)	CSG Solar (< 2 µm on glass) [6]
III–V cells							
GaAs (thin-film cell)	29.1 ± 0.6	0.998 (ap)	1.1272	29.78[f]	86.7	FhG-ISE (10/18)	Alta Devices [7]
GaAs (multicrystalline)	18.4 ± 0.5	4.011 (t)	0.994	23.2	79.7	NREL (11/95)	RTI, Ge substrate [8]
InP (crystalline cell)	24.2 ± 0.5[g]	1.008 (ap)	0.939	31.15[h]	82.6	NREL (3/13)	NREL [9]
Thin film chalcogenide							
CIGS (cell) (Cd-free)	23.35 ± 0.5	1.043 (da)	0.734	39.58[i]	80.4	AIST (11/18)	Solar Frontier [10]
CIGSSe (submodule)	20.3 ± 0.4	526.7 (ap)	0.6834	39.55[c,j]	75.1	NREL (5/23)	Avancis, 100 cells [11]
CdTe (cell)	21.0 ± 0.4	1.0623 (ap)	0.8759	30.25[d]	79.4	Newport (8/14)	First Solar, on glass [12]
CZTSSe (cell)	13.45 ± 0.3	1.101 (da)	0.5109	37.90[k]	69.5	NPVM (4/24)	IoP/CAS [13]
CZTSSe (minimodule)	**11.95 ± 0.3**	**10.47 (da)**	**0.5073[c]**	**34.82[c,b]**	**67.7**	**NPVM (9/24)**	**IoP/CAS, 4 cells** [13]
CZTS (cell)	10.0 ± 0.2	1.113 (da)	0.7083	21.77[h]	65.1	NREL (3/17)	UNSW [14]
Amorphous/microcrystalline							
Si (amorphous cell)	10.2 ± 0.3[g,l]	1.001 (da)	0.896	16.36[d]	69.8	AIST (7/14)	AIST [15]
Si (microcrystalline cell)	11.9 ± 0.3[g]	1.044 (da)	0.550	29.72[h]	75.0	AIST (2/17)	AIST [16]
Perovskite							
Perovskite (cell)	25.2 ± 0.8[m]	1.0347 (da)	1.162	26.39[j]	82.0	Newport (7/23)	NorthwesternU [17]
Perovskite (minimodule)	**23.2 ± 0.5[m]**	**20.25 (da)**	**1.185[c]**	**24.31[c,b]**	**80.5**	**NPVM (9/24)**	**NUS/SERIS, 8 cells** [18]
Perovskite (submodule)	**20.6 ± 0.7[m]**	**215.53 (da)**	**1.185[c]**	**22.22[c,b]**	**78.3**	**FhG-ISE (4/24)**	**KRICT/UniTest, 29 cells** [19]
Dye sensitized							
Dye (cell)	11.9 ± 0.4[n]	1.005 (da)	0.744	22.47[o]	71.2	AIST (9/12)	Sharp [20,21]
Dye (minimodule)	10.7 ± 0.4[n]	26.55 (da)	0.754[c]	20.19[c,p]	69.9	AIST (2/15)	Sharp, 7 serial cells [20,21]

(Continues)

TABLE 1 | (Continued)

Classification	Efficiency (%)	Area (cm^2)	V_{oc} (V)	J_{sc} (mA/cm^2)	Fill factor (%)	Test centre (date)	Description
Dye (submodule)	8.8 ± 0.3[n]	398.8 (da)	0.697[c]	18.42[c,q]	68.7	AIST (9/12)	Sharp, 26 serial cells [20,21]
Organic							
Organic (cell)	15.8 ± 0.3[g,r]	1.064 (da)	0.8513	25.11[k]	73.9	FhG-ISE (6/23)	Fraunhofer ISE/FMF [22]
Organic (minimodule)	15.7 ± 0.3[r]	19.31 (da)	0.8771[c]	24.37[c,j]	73.4	JET (1/23)	ZhejiangU, 7 cells [23]
Organic (submodule)	14.5 ± 0.2[r]	204.11 (da)	0.8315[c]	23.32[c,k]	74.6	FhG-ISE (11/23)	FAU/FZJ, 38 cells [24]

Abbreviations: (ap) = aperture area, (da) = designated illumination area, (t) = total area, AIST = Japanese National Institute of Advanced Industrial Science and Technology, a-Si = amorphous silicon/hydrogen alloy, CIGS = $CuIn_{1-y}Ga_ySe_2$, CZTS = Cu_2ZnSnS_4, CZTSSe = $Cu_2ZnSnS_{4-y}Se_y$, FhG-ISE = Fraunhofer Institut für Solare Energiesysteme, ISFH = Institute für Solarenergieforschung, JET = Japan Electrical Safety and Environment Technology Laboratories, nc-Si = nanocrystalline or microcrystalline silicon, NPVM = Chinese National Photovoltaic Industry Measurement and Testing Center, NREL = US National Renewable Energy Laboratory.

[a]Contacting: Front: Unmetallized; Rear: Rear: 2x9BB, busbar resistance neglecting (brn) contacting, highly reflective (white) chuck (hrc).
[b]Spectral response and current–voltage curve reported in the present version of these tables.
[c]Reported on a 'per cell' basis.
[d]Spectral responses and current–voltage curve reported in Version 45 of these tables.
[e]Recalibrated from original measurement.
[f]Spectral response and current–voltage curve reported in Version 53 of these tables.
[g]Not measured at an external laboratory.
[h]Spectral response and current–voltage curve reported in Version 50 of these tables.
[i]Spectral response and current–voltage curve reported in Version 54 of these tables.
[j]Spectral response and current–voltage curve reported in Version 62 of these tables.
[k]Spectral response and current–voltage curve reported in Version 64 of these tables.
[l]Stabilized by 1000-h exposure to 1 sunlight at 50°C.
[m]Initial performance. References [25] and [26] review the stability of similar devices.
[n]Initial efficiency. Reference [27] reviews the stability of similar devices.
[o]Spectral response and current–voltage curve reported in Version 41 of these tables.
[p]Spectral response and current–voltage curve reported in Version 46 of these tables.
[q]Spectral response and current–voltage curve reported in Version 43 of these tables.
[r]Initial performance. References [28] and [29] review the stability of similar devices.

TABLE 2 | 'Notable Exceptions' for single-junction cells and submodules: 'Top dozen' confirmed results, not class records, measured under the global AM1.5 spectrum (1000 Wm^{-2}) at 25°C (IEC 60904-3: 2008 or ASTM G-173-03 global).

Classification	Efficiency (%)	Area (cm^2)	V_{oc} (V)	J_{sc} (mA/cm^2)	Fill factor (%)	Test centre (date)	Description
Cells (silicon)							
Si	25.0 ± 0.5	4.00 (da)	0.706	42.7[a]	82.8	Sandia (3/99)	UNSW, p-type PERC [30]
Si	25.8 ± 0.5[b]	4.008 (da)	0.7241	42.87[c]	83.1	FhG-ISE (7/17)	FhG-ISE, n-type TOPCon [31]
Si	26.0 ± 0.5[b]	4.015 (da)	0.7323	42.05[d]	84.3	FhG-ISE (11/19)	FhG-ISE, p-type TOPCon
Si	26.1 ± 0.3[b]	3.9857 (da)	0.7266	42.62[e]	84.3	ISFH (2/18)	ISFH, p-type TBC [32]
Si (large)	24.0 ± 0.3[f]	244.59 (t)	0.6940	41.58[g]	83.3	ISFH (7/19)	LONGi, p-type PERC [33]
Si (large)	**25.9 ± 0.4**[h]	**350.5 (t)**	**0.7383**	**41.70**[i]	**84.1**	**ISFH (10/24)**	**TRINA, n-type TOPCon** [34]
Si (large)	**27.0 ± 0.5**[j]	**350.0 (t)**	**0.7447**	**42.32**[k]	**85.8**	**ISFH (8/24)**	**LONGi, n-type TBC** [4]
Si (large)	26.8 ± 0.4[l]	274.4 (t)	0.7514	41.45[m]	86.1	ISFH (10/22)	LONGi, n-type HJT [35]
Si (large)	26.6 ± 0.4[l]	274.1 (t)	0.7513	41.30[m]	85.6	ISFH (10/22)	LONGi, p-type HJT [36]
Si (large)	**27.3 ± 0.4**[n]	**243.1 (da)**	**0.7434**	**42.60**[k]	**86.2**	**ISFH (12/23)**	**LONGi, n-type HBC** [4]
GaInP	22.0 ± 0.3[b]	0.2502 (ap)	1.4695	16.63[o]	90.2	NREL (1/19)	NREL, rear HJ, strained AlInP [37]
Cells (chalcogenide)							
CIGS (thin-film)	23.6 ± 0.4	0.899 (da)	0.7671	38.30[p]	80.5	FhG-ISE (1/23)	Evolar/UppsalaU [38]
CdTe (thin-film)	**23.1 ± 0.3**	**0.4507 (da)**	**0.9048**	**31.66**[k]	**80.6**	**NREL (5/24)**	**First Solar** [39]
CZTSSe (thin-film)	15.1 ± 0.3	0.2697 (da)	0.5299	38.44[i]	74.0	NPVM (4/24)	IoP/CAS [13]
CZTS (thin-f; >1.5 eV)	**13.2 ± 0.3**	**0.2021 (da)**	**0.7490**	**23.40**[k]	**68.9**	**NPVM (5/24)**	**UNSW (Cd-free)** [40]
$Sb_2(S,Se)_3$	**10.7 ± 0.4**	**0.0389 (da)**	**0.6345**	**24.55**[k]	**68.6**	**CSIRO (10/24)**	**UNSW**
Cells (other)							
Perovskite (thin-film)	26.7 ± 0.6[q,r]	0.0519 (da)	1.193	26.49[i]	84.5	NPVM (5/24)	USTC [41]
Organic (thin-film)	19.2 ± 0.3[s]	0.0326 (da)	0.9135	26.61[p]	79.0	NREL (3/23)	SJTU [42]
Dye sensitized	13.0 ± 0.4[t]	0.1155 (da)	1.0396	15.55[p]	80.4	FhG-ISE (10/20)	EPFL [43]

Abbreviations: (ap) = aperture area, (da) = designated illumination area, (t) = total area, AIST = Japanese National Institute of Advanced Industrial Science and Technology, CIGS = $CuIn_{1-y}Ga_ySe_2$, CZTS = Cu_2ZnSnS_4, CZTSSe = $Cu_2ZnSnS_{4-y}Se_y$, FhG-ISE = Fraunhofer-Institut für Solare Energiesysteme, ISFH = Institute for Solar Energy Research, Hamelin, NREL = National Renewable Energy Laboratory.
[a]Spectral response reported in Version 36 of these tables.
[b]Not measured at an external laboratory.
[c]Spectral response and current–voltage curves reported in Version 51 of these tables.
[d]Spectral response and current–voltage curves reported in Version 55 of these tables.
[e]Spectral response and current–voltage curve reported in Version 52 of these tables.
[f]Contacting: Front: 12BB, resistance neglecting (brn); Rear: fully metallized, full area contacting (fac).
[g]Spectral response and current–voltage curves reported in Version 57 of these tables.
[h]Contacting: 16BB, busbar resistance neglecting (brn); Rear: 16BB, grid resistance neglecting (grn) contacting, full area contacting (fac).
[i]Spectral response and current–voltage curve reported in Version 64 of these tables.
[j]Contacting: Front: Unmetallized; Rear: Rear: 2x9BB, busbar resistance neglecting (brn) contacting, highly reflective (white) chuck (hrc).
[k]Spectral response and current–voltage curves reported in the present version of these tables.
[l]Contacting: Front: 12BB, busbar resistance neglecting (brn) contacting; Rear: 12BB, grid resistance neglecting (grn) contacting, highly reflective chuck (hrc).
[m]Spectral response and current–voltage curves reported in Version 61 of these tables.
[n]Contacting: Front: Unmetallized; Rear: Rear: 2x6BB, busbar resistance neglecting (brn) contacting, highly reflective (white) chuck (hrc).
[o]Spectral response and current–voltage curve reported in Version 54 of these tables.
[p]Spectral response and current–voltage curves reported in Version 62 of these tables.
[q]Stability not investigated. References [25] and [26] document stability of similar devices.
[r]Measured using a 10-point IV sweep with constant voltage bias until current change rate <0.07%/min.
[s]Long-term stability not investigated. References [28] and [29] document stability of similar devices.
[t]Long-term stability not investigated. Reference [27] documents stability of similar devices.

TABLE 3 | Confirmed multiple-junction terrestrial cell and submodule efficiencies measured under the global AM1.5 spectrum (1000 W/m^2) at 25°C (IEC 60904-3: 2008 or ASTM G-173-03 global).

Classification	Efficiency (%)	Area (cm^2)	V_{oc} (V)	J_{sc} (mA/cm^2)	Fill factor (%)	Test centre (date)	Description
III–V multijunctions							
5 junction cell (bonded) (2.17/1.68/1.40/1.06/.73 eV)	38.8 ± 1.2	1.021 (ap)	4.767	9.564	85.2	NREL (7/13)	Spectrolab, 2-terminal
InGaP/GaAs/InGaAs	37.9 ± 1.2	1.047 (ap)	3.065	14.27[a]	86.7	AIST (2/13)	Sharp, 2 term [44].
GaInP/GaAs (monolithic)	32.8 ± 1.4	1.000 (ap)	2.568	14.56[b]	87.7	NREL (9/17)	LG Electronics, 2 term.
III-V/Si multijunctions							
GaInP/GaInAsP//Si (bonded)	36.1 ± 1.3[c]	3.987 (ap)	3.309	12.70[d]	86.0	FhG-ISE (5/23)	FhG-ISE/AMOLF, 2-term [45].
GaInP/GaAs/Si (mech. stack)	35.9 ± 0.5[c]	1.002 (da)	2.52/0.681	13.6/11.0	87.5/78.5	NREL (2/17)	NREL/CSEM/EPFL, 4-term [46].
GaInP/GaAs/Si (monolithic)	25.9 ± 0.9[c]	3.987 (ap)	2.647	12.21[e]	80.2	FhG-ISE (6/20)	Fraunhofer ISE, 2-term [47].
GaAsP/Si (monolithic)	23.4 ± 0.3	1.026 (ap)	1.732	17.34[f]	77.7	NREL (5/20)	OSU/UNSW/SolAero, 2-term [48]
GaAs/Si (mech. stack)	32.8 ± 0.5[c]	1.003 (da)	1.09/0.683	28.9/11.1[g]	85.0/79.2	NREL (12/16)	NREL/CSEM/EPFL, 4-term [46].
GaInP/GaInAs/Ge; Si (spectral split minimodule)	34.5 ± 2.0	27.83 (ap)	2.66/0.65	13.1/9.3	85.6/79.0	NREL (4/16)	UNSW/Azur/Trina, 4-term [49].
Perov./Si multijunctions							
Perovskite/Si	**34.6 ± 1.0**[h]	**1.0044 (da)**	**1.996**	**20.71**[i]	**83.6**	**ESTI (5/24)**	**LONGi, 2-term** [50].
Perovskite/Si (large)	**30.1 ± 1.3**[h]	**212.1(ap)**	**1.997**	**19.69**[i]	**76.5**	**FhG-ISE (5/23)**	**LONGi, 2-term** [50].
Other multijunctions							
Perovskite/CIGS	24.2 ± 0.7[h]	1.045 (da)	1.768	19.24[f]	72.9	FhG-ISE (1/20)	HZB, 2-terminal [51]
Perovskite/perovskite	28.2 ± 0.5[h]	1.038 (da)	2.159	16.59[j]	78.9	JET (12/22)	NanjingU/Renshine, 2-term [52].
Perovskite/perovskite (minimodule)	**24.8 ± 0.6**[h]	**64.98 (da)**	**2.134**	**15.32**[i]	**75.9**	**JET (12/23)**	**NanjingU/Renshine, 14 cells** [53]
a-Si/nc-Si/nc-Si (thin-film)	14.0 ± 0.4[c,k]	1.045 (da)	1.922	9.94[l]	73.4	AIST (5/16)	AIST, 2-term [54].
a-Si/nc-Si (thin-film cell)	12.7 ± 0.4[c,k]	1.000 (da)	1.342	13.45[m]	70.2	AIST (10/14)	AIST, 2-term [55].
'Notable exceptions'							
GaInP/GaAs (mqw)	32.9 ± 0.5[c]	0.250 (ap)	2.500	15.36[n]	85.7	NREL (1/20)	NREL/UNSW, multiple QW
GaInP/GaAs/GaInAs	37.8 ± 1.4	0.998 (ap)	3.013	14.60[n]	85.8	NREL (1/18)	Microlink (ELO) [56]
GaInP/GaAs (mqw)/GaInAs	39.5 ± 0.5[c]	0.242 (ap)	2.997	15.44[o]	85.3	NREL (9/21)	NREL, multiple QW

(Continues)

TABLE 3 | (Continued)

Classification	Efficiency (%)	Area (cm^2)	V_{oc} (V)	J_{sc} (mA/cm^2)	Fill factor (%)	Test centre (date)	Description
6 junction (monolithic) (2.19/1.76/1.45/1.19/0.97/.7 eV)	39.2 ± 3.2[c]	0.247 (ap)	5.549	8.457[p]	83.5	NREL (11/18)	NREL, inv. metamorphic [57]
GaInP/AlGaAs/CIGS	28.1 ± 1.2[c]	0.1386 (da)	2.952	11.72[q]	81.1	AIST (1/21)	AIST/FhG-ISE, 2-term [58].
Perovskite/perovskite	30.1 ± 0.8[h]	0.0493 (da)	2.20	16.72[r]	81.8	JET (10/23)	NanjingU/Renshine, 2-term [52].
Perovskite/organic	**25.1 ± 0.8[h]**	**0.0347 (da)**	**2.159**	**14.38[i]**	**80.8**	**JET (5/24)**	**HarvSolar/CityU-HK, 2-term** [59].

Abbreviations: (ap) = aperture area, (da) = designated illumination area, (t) = total area, AIST = Japanese National Institute of Advanced Industrial Science and Technology, a-Si = amorphous silicon/hydrogen alloy, ESTI = European Solar Test Installation, FhG-ISE = Fraunhofer Institut für Solare Energiesysteme, JET = Japan Electrical Safety and Environment Technology Laboratories, nc-Si = nanocrystalline or microcrystalline silicon, NREL = US National Renewable Energy Laboratory.

[a]Spectral response and current–voltage curve reported in Version 42 of these tables.
[b]Spectral response and current–voltage curve reported in the Version 51 of these tables.
[c]Not measured at an external laboratory.
[d]Spectral response and current–voltage curves reported in the present version of these tables.
[e]Spectral response and current–voltage curve reported in Version 57 of these tables.
[f]Spectral response and current–voltage curve reported in Version 56 of these tables.
[g]Spectral response and current–voltage curve reported in Version 52 of these tables.
[h]Initial efficiency. References [25] and [26] review the stability of similar perovskite-based devices.
[i]Spectral response and current–voltage curves reported in the present version of these tables.
[j]Spectral response and current–voltage curve reported in Version 63 of these tables.
[k]Stabilized by 1000-h exposure to 1 sunlight at 50°C.
[l]Spectral response and current–voltage curve reported in Version 49 of these tables.
[m]Spectral responses and current–voltage curve reported in Version 45 of these tables.
[n]Spectral response and current–voltage curve reported in Version 53 of these tables.
[o]Spectral response and current–voltage curves reported in Version 59 of these tables.
[p]Spectral response and current–voltage curve reported in Version 54 of these tables.
[q]Spectral response and current–voltage curve reported in Version 58 of these tables.
[r]Spectral response and current–voltage curve reported in Version 64 of these tables.

TABLE 4 | Confirmed nonconcentrating terrestrial module efficiencies measured under the global AM1.5 spectrum (1000 W/m^2) at a cell temperature of 25°C (IEC 60904-3: 2008 or ASTM G-173-03 global).

Classification	Effic. (%)	Area (cm^2)	V_{oc} (V)	I_{sc} (A)	FF (%)	Test centre (date)	Description
Si (crystalline)	**25.4 ± 0.3**	**18,342 (da)**	**40.30**	**13.873[a]**	**83.4**	**NREL (7/24)**	**LONGi** [4]
GaAs (thin-film)	25.1 ± 0.8	866.45 (ap)	11.08	2.303[b]	85.3	FhG-ISE (11/17)	Alta Devices [60]
CIGS (Cd-free)	19.2 ± 0.5	841 (ap)	48.0	0.456[c]	73.7	AIST (1/17)	Solar Frontier (70 cells) [61]
CdTe (thin-film)	19.9 ± 0.3	23,932 (da)	231.5	2.675[a]	77.1	NREL (6/23)	First Solar [62]
Perovskite	19.2 ± 0.4[d]	1027 (da)	59.4	0.4307[a]	77.1	NREL (12/23)	SolaEon [63]
Organic	13.1 ± 0.3[e]	1475 (da)	48.10	0.6015[f]	67.0	NREL (5/23)	Waystech/ Nanobit [64]
Multijunction							
InGaP/GaAs/ InGaAs	32.65 ± 0.7	965 (da)	24.30	1.520[g]	85.3	AIST (2/22)	Sharp (40 cells; 8 series) [65]
Perovskite/Si	**26.9 ± 1.0[d]**	**16,023 (da)**	**56.18**	**9.456**	**81.1**	**FhG-ISE (6/24)**	**Oxford PV** [66]
a-Si/nc-Si (tandem)	12.3 ± 0.3[h]	14,322 (t)	280.1	0.902[i]	69.9	ESTI (9/14)	TEL Solar, Trubbach Labs [67]
'Notable Exceptions'							
CIGS (large)	18.6 ± 0.6	10,858 (ap)	58.00	4.545[j]	76.8	FhG-ISE (10/19)	Miasole [68]
InGaP/GaAs//Si	33.7 ± 0.7	775 (da)	20.3/2.83	1.25/1.93[f]	86.5/78.0	AIST (2/23)	Sharp/Toyota TI, 4-term [69].
InGaP/GaAs// CIGS	31.2 ± 0.7	778 (ap)	20.3/16.9	1.24/.26[f]	85.7/59.8	AIST (2/23)	Sharp/Idemitsu, 4-term [69].
Perovskite (large)	**17.2 ± 0.5[d]**	**7200 (t)**	**103.5**	**1.579[a]**	**75.6**	**NREL (8/24)**	**Renshine** [70]

Abbreviations: (ap) = aperture area, (da) = designated illumination area, (t) = total area, a-Si = amorphous silicon/hydrogen alloy, a-SiGe = amorphous silicon/germanium/hydrogen alloy, CIGSS = CuInGaSSe, Effic. = efficiency, FF = fill factor, nc-Si = nanocrystalline or microcrystalline silicon.
[a]Spectral response and current–voltage curve reported in the present version of these tables.
[b]Spectral response and current–voltage curve reported in Version 51 of these tables.
[c]Spectral response and current–voltage curve reported in Version 50 of these tables.
[d]Initial performance. References [25] and [26] review the stability of similar devices.
[e]Initial performance. References [28] and [29] review the stability of similar devices.
[f]Spectral response and current voltage curve reported Version 62 of these tables.
[g]Spectral response and current–voltage curve reported in Version 60 of these tables.
[h]Stabilized at the manufacturer to the 2% level following IEC procedure of repeated measurements.
[i]Spectral response and/or current–voltage curve reported in Version 46 of these tables.
[j]Spectral response and current–voltage curve reported in Version 55 of these tables.

Table 2 contains what might be described as 'notable exceptions' for 'one-sun' single-junction cells and submodules in the above category. Although not conforming to the requirements to be recognized as a class record, the devices in Table 2 have notable characteristics that will be of interest to sections of the photovoltaic community, with entries based on their significance and timeliness. To encourage discrimination, the table is limited to nominally 15 entries with the present authors having voted for their preferences for inclusion. Readers who have suggestions for notable exceptions for inclusion into this or subsequent tables are welcome to contact any of the authors with full details. Suggestions conforming to the guidelines will be included on the voting list for a future issue.

Table 3 was first introduced in Version 49 of these tables and summarizes the growing number of cell and submodule results involving high efficiency, one-sun multiple-junction devices (previously reported in Table 1). Table 4 shows the best results for one-sun modules, both single- and multiple-junction, whereas Table 5 shows the best results for concentrator cells and concentrator modules. A small number of 'notable exceptions' are also included in Tables 3–5.

2 | New Results

Seventeen new results are reported in the present version of these tables. The first is the very first entry reported in Table 1

TABLE 5 | Terrestrial concentrator cell and module efficiencies measured under the ASTM G-173-03 direct beam AM1.5 spectrum at a cell temperature of 25°C (except where noted for the hybrid and luminescent modules).

Classification	Effic. (%)	Area (cm^2)	Intensity[a] (suns)	Test centre (date)	Description
Single cells					
GaAs	30.8 ± 1.9[b,c]	0.0990 (da)	61	NREL (1/22)	NREL, 1 junction (1 J)
Si	27.6 ± 1.2[d]	1.00 (da)	92	FhG-ISE (11/04)	Amonix back-contact [71]
CIGS (thin-film)	23.3 ± 1.2[b,e]	0.09902 (ap)	15	NREL (3/14)	NREL [72]
Multijunction cells					
AlGaInP/AlGaAs/GaAs/GaInAs(3) (2.15/1.72/1.41/1.17/0.96/0.70 eV)	47.1 ± 2.6[b,f]	0.099 (da)	143	NREL (3/19)	NREL, 6 J inv. metamorphic [57]
GaInP/GaInAs; GaInAsP/GaInAs	47.6 ± 2.6[b,g]	0.0452 (da)	665	FhG-ISE (5/22)	FhG-ISE 4 J bonded [73]
GaInP/GaAs/GaInAs/GaInAs	45.7 ± 2.3[b,h]	0.09709 (da)	234	NREL (9/14)	NREL, 4 J monolithic [74]
InGaP/GaAs/InGaAs	44.4 ± 2.6[i]	0.1652 (da)	302	FhG-ISE (4/13)	Sharp, 3 J inverted metamorphic [75]
GaInAsP/GaInAs	35.5 ± 1.2[b,j]	0.10031 (da)	38	NREL (10/17)	NREL 2-junction (2 J) [76]
Minimodule					
GaInP/GaAs; GaInAsP/GaInAs	43.4 ± 2.4[b,k]	18.2 (ap)	340[l]	FhG-ISE (7/15)	Fraunhofer ISE 4 J (lens/cell) [77]
Submodule					
GaInP/GaInAs/Ge; Si	40.6 ± 2.0[k]	287 (ap)	365	NREL (4/16)	UNSW 4 J split spectrum [78]
Modules					
Si	20.5 ± 0.8[b]	1875 (ap)	79	Sandia (4/89)[l]	Sandia/UNSW/ENTECH (12 cells) [79]
Three junction (3 J)	35.9 ± 1.8[m]	1092 (ap)	N/A	NREL (8/13)	Amonix [80]
Four junction (4 J)	38.9 ± 2.5[n]	812.3 (ap)	333	FhG-ISE (4/15)	Soitec [81]
Hybrid module[o]					
4-Junction (4 J)/bifacial c-Si	34.2 ± 1.9[b,o]	1088 (ap)	CPV/PV	FhG-ISE (9/19)	FhG-ISE (48/8 cells; 4 T) [82]
'Notable exceptions'					
Si (large area)	21.7 ± 0.7	20.0 (da)	11	Sandia (9/90)[l]	UNSW laser grooved [83]
Luminescent minimodule[o]	7.1 ± 0.2	25 (ap)	2.5[p]	ESTI (9/08)	ECN Petten, GaAs cells [84]
4J minimodule	41.4 ± 2.6[b]	121.8 (ap)	230	FhG-ISE (9/18)	FhG-ISE, 10 cells [85]

Note: Following the normal convention, efficiencies calculated under this direct beam spectrum neglect the diffuse sunlight component that would accompany this direct spectrum. These direct beam efficiencies need to be multiplied by a factor estimated as 0.8746 to convert to thermodynamic efficiencies [86].
Abbreviations: (ap) = aperture area, (da) = designated illumination area, CIGS = $CuInGaSe_2$, Effic. = efficiency, ESTI = European Solar Test Installation, FhG-ISE = Fraunhofer-Institut für Solare Energiesysteme, NREL = National Renewable Energy Laboratory.
[a]One sun corresponds to direct irradiance of 1000 Wm^{-2}.
[b]Not measured at an external laboratory.
[c]Spectral response and current–voltage curve reported in Version 60 of these tables.
[d]Measured under a low aerosol optical depth spectrum similar to ASTM G-173-03 direct [87].
[e]Spectral response and current–voltage curve reported in Version 44 of these tables.
[f]Spectral response and current–voltage curve reported in Version 54 of these tables.
[g]Spectral response and current–voltage curve reported in Version 61 of these tables.
[h]Spectral response and current–voltage curve reported in Version 46 of these tables.
[i]Spectral response and current–voltage curve reported in Version 42 of these tables.
[j]Spectral response and current–voltage curve reported in Version 51 of these tables.
[k]Determined at IEC 62670-1 CSTC reference conditions.
[l]Recalibrated from original measurement.
[m]Referenced to 1000 W/m^2 direct irradiance and 25°C cell temperature using the prevailing solar spectrum and an in-house procedure for temperature translation.
[n]Measured under IEC 62670-1 reference conditions following the current IEC power rating draft 62670-3.
[o]Thermodynamic efficiency. Hybrid and luminescent modules measured under the ASTM G-173-03 or IEC 60904-3: 2008 global AM1.5 spectrum at a cell temperature of 25°C. 4-terminal module with external dual-axis tracking. The power rating of CPV follows the IEC 62670-3 standard; front power rating of flat plate PV based on IEC 60904-3, -5, -7, -10, and 60891 with modified current translation approach; rear power rating of flat plate PV based on IEC TS 60904-1, -2, and 60891.
[p]Geometric concentration.

('one-sun cells and submodules'). An efficiency of 27.4% is reported for a large-area (166 cm^2; half-cut M10 wafer) n-type silicon hybrid interdigitated-back-contact (HTBC) cell, with rear heterojunction (HJT) p-type contacts and rear TOPCon n-type contacts, fabricated by LONGi Solar [4] and measured by the Institute für Solarenergieforschung (ISFH). The cell, establishing a new outright record for silicon, has both polarity contacts on the rear surface, as already noted, restricting loss by the absence of contacts on the front illuminated surface.

The second new result is 11.95% efficiency for a 10 cm^2 $Cu_2ZnSnS_ySe_{4-y}$ (CZTSSe) shingled minimodule fabricated by the Institute of Physics, Chinese Academy of Sciences (IoP/CAS) [13] and measured by the Chinese National Photovoltaic Industry Measurement and Testing Center (NPVM). A third new result is 23.2% efficiency for a small area (20-cm^2) lead halide perovskite minimodule consisting of eight cells connected in series, with the minimodule fabricated by the National University of Singapore (NUS) in conjunction with the Solar Energy Research Institute of Singapore (SERIS) [18] and again measured by NPVM. The final new result in table is a new record of 20.6% for a much larger 216-cm^2 lead halide perovskite submodule [19] consisting of 29 serially connected cells, fabricated by the Korea Research Institute of Chemical Technology (KRICT) in conjunction with and Korean semiconductor equipment maker UniTest and measured by the Fraunhofer Institute for Solar Energy Systems (FhG-ISE).

Six new results are also reported in Table 2 (one-sun 'notable exceptions'). The first is an efficiency of 25.9% for a very large area (350.5 cm^2, the largest in these tables), silicon n-type TOPCon (tunnel oxide passivated contact) cell fabricated by Trina Solar and measured by ISFH. The second is an efficiency of 27.0% for a similarly large area (350 cm^2) silicon n-type TOPCon interdigitated back contact (TBC) cell [34] fabricated by LONGi Solar and measured by ISFH. The third is the movement of the result for the 27.3% efficient,large-area n-type silicon cell also fabricated by LONGi Solar in 2023 from Table 1 to Table 2, notable as it is the most efficient, all-HJT interdigitated back contact (HBC) solar cell.

The next two results involve small area (< 1-cm^2) chalcogenide thin-film solar cells. The first is an increase in efficiency to 23.1% for a small area (0.45-cm^2) CdTe-based cell fabricated by First Solar [39] and measured by NREL, improving on the 22.6% result first reported in the previous version of these tables [1]. The second new chalcogenide result is for a nominally pure-sulfide CZTS solar cell with efficiency increased to 13.2%

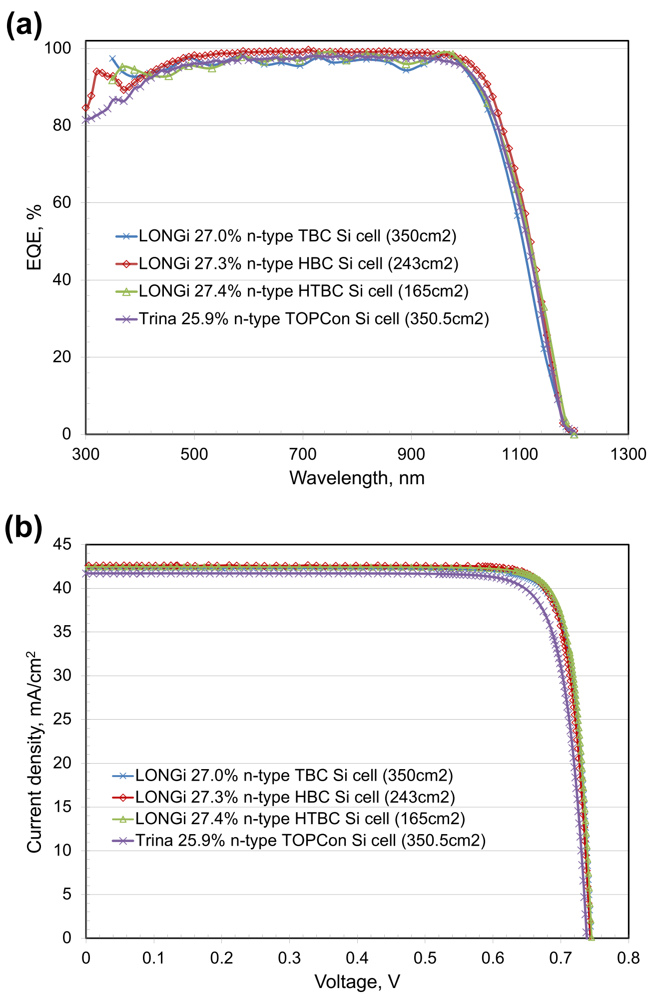

FIGURE 1 | (a) External quantum efficiency (EQE) for the new silicon cell results reported in this issue (some curves are normalized). (b) Corresponding current density–voltage (JV) curves.

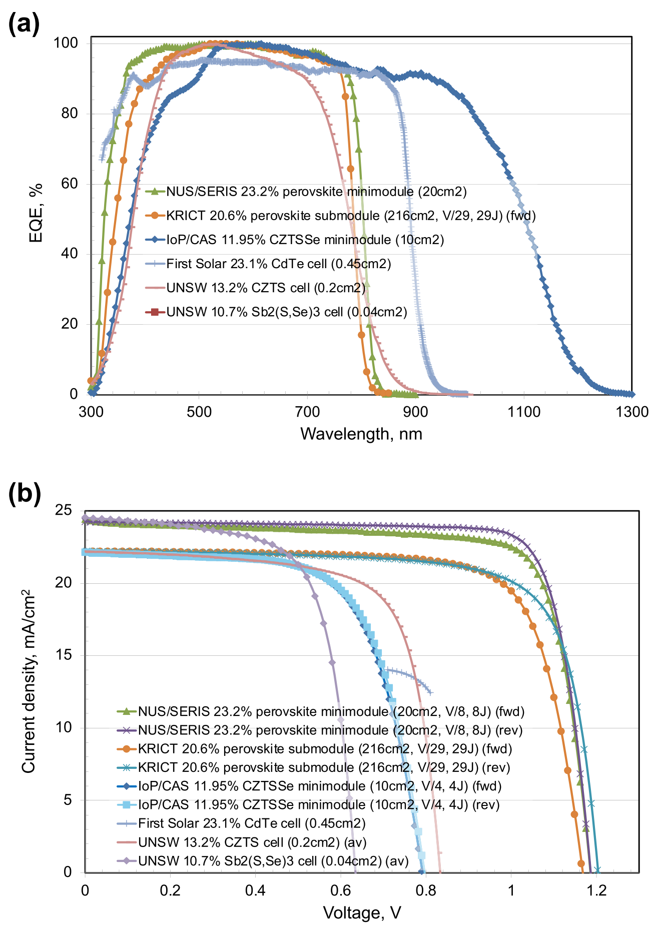

FIGURE 2 | (a) External quantum efficiency (EQE) for new thin-film cell, minimodule and submodule results reported in this issue (some curves are normalized). (b) Corresponding current density–voltage (JV) curves.

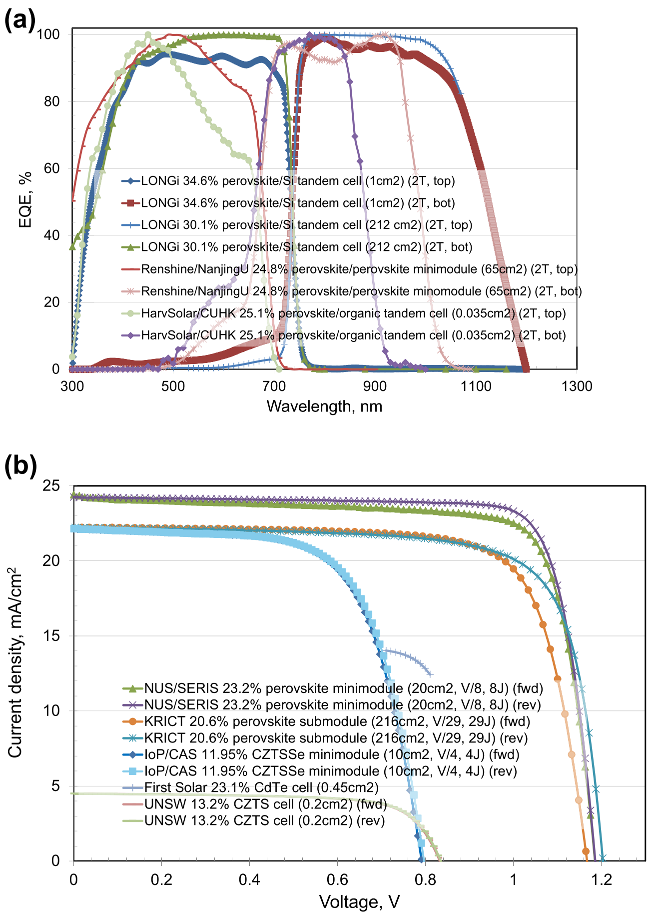

FIGURE 3 | (a) External quantum efficiency (EQE) for new 2-terminal double-junction cell and minimodule results reported in this issue (results are normalized). (b) Corresponding current density–voltage (JV) curves.

for a small-area (0.2-cm^2) cell fabricated by the University of New South Wales (UNSW), Sydney, and measured at NPVM. Because various alloying agents can reduce the bandgap (E_g) of this material, leading to an efficiency increase, future entries will be restricted to $E_g > 1.5$ eV, as determined from the maximum slope of the EQE curve. The final new result in Table 2 creates a new chalcogenide category, with over 10% efficiency confirmed for an antimony sulphide selenide cell. An efficiency of 10.7% was measured for a 0.04-cm^2 $Sb_2(S,Se)_3$ cell fabricated at the University of New South Wales, Sydney (UNSW), and measured by the Commonwealth Scientific and Industrial Research Organization (CSIRO). For these last three results, cell area is too small for classification as an outright record, with solar cell efficiency targets in governmental research programs generally specified in terms of a cell area of 1 cm^2 or larger [88–90].

There are also four new results reported in Table 3 describing results for one-sun, multijunction devices—all involving perovskites in tandem cells. An efficiency of 34.6% is reported for a 1 cm^2, 2-terminal, silicon/perovskite tandem cell fabricated by LONGi Central R&D Institute and measured at the European Solar Test Installation (ESTI) at the European Commission's Joint Research Centre, Ispra, beating out LONGi's earlier 34.2% result. The second is an efficiency of 30.1% for a much larger

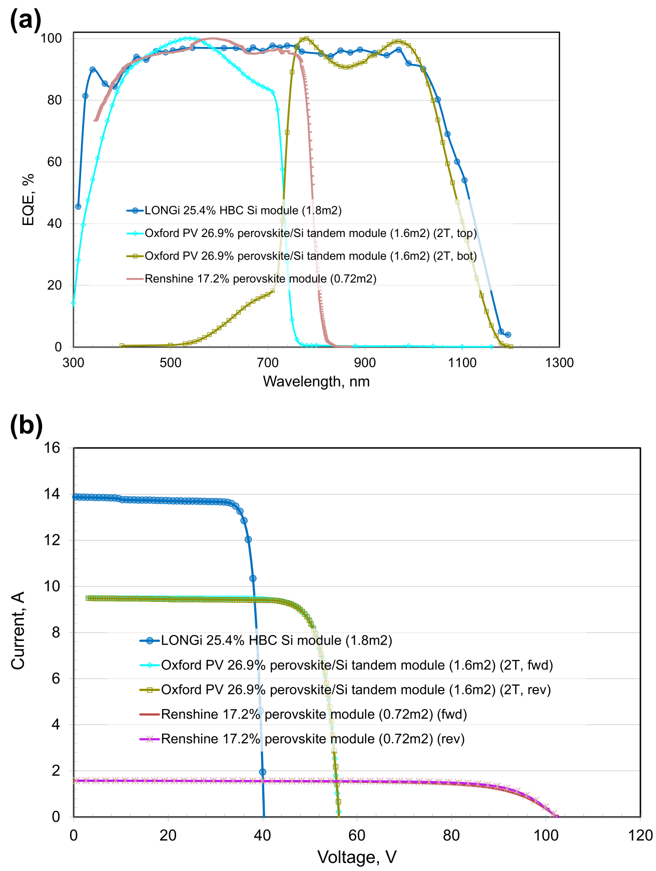

FIGURE 4 | (a) External quantum efficiency (EQE) for the new module results reported in this issue. (b) Corresponding current density–voltage (JV) curves.

area (212-cm^2), 2-terminal, silicon/perovskite tandem cell again fabricated by LONGi and measured by FhG-ISE.

The third new result in Table 3 is 24.8% efficiency for a 65-cm^2, perovskite/perovskite tandem cell minimodule fabricated by Nanjing University and Renshine Solar (Suzhou) Co., Ltd. and measured by the Japan Electrical Safety and Environment Technology Laboratories (JET). The final new result in this table as a 'notable exception' is 25.1% for a very small area (0.035-cm^2) perovskite/organic 2-terminal tandem cell again fabricated by HarvSolar and the City University of Hong Kong (CityU-HK) and again measured by JET.

There are three new results reported in Table 4 (one-sun modules) involving a range of commercially sized silicon and perovskite technologies. The first is a new efficiency level of 25.4% reported for a 1.8-m^2 silicon module [60] fabricated by LONGi and measured by NREL. The second result is a new record of 26.9% efficiency for a 1.6-m^2 silicon/perovskite tandem cell module fabricated by Oxford PV and measured by FhG-ISE. The third is an improvement to 17.2% efficiency for a 0.72-m^2 perovskite thin-film module [64] fabricated by Renshine and again measured by NREL.

The EQE spectra for the new silicon cells reported in the present issue of these tables are shown in Figure 1a, with Figure 1b showing the current density–voltage (JV) curves for the same devices. Figure 2a,b shows the corresponding EQE and JV curves for several of the new thin-film cell, minimodule and submodule results. Figure 3a,b shows these for the new 2-terminal double-junction tandem cell and minimodule results, whereas Figure 4a,b shows these for the new module results.

Acknowledgements

The Australian Centre for Advanced Photovoltaics commenced operation in February 2013 with support from the Australian Government through the Australian Renewable Energy Agency (ARENA). The Australian Government does not accept responsibility for the views, information or advice expressed herein. The work at NREL was supported by the U.S. Department of Energy under Contract No. DE-AC36-08-GO28308 with the National Renewable Energy Laboratory. The work at AIST was supported in part by the Japanese New Energy and Industrial Technology Development Organisation (NEDO) under the Ministry of Economy, Trade and Industry (METI).

Data Availability Statement

The data that support the findings of this study are available from the corresponding author upon reasonable request.

Disclaimer

Although the information provided in the tables is provided in good faith, the authors, editors and publishers cannot accept direct responsibility for any errors or omissions.

References

1. M. A. Green, E. D. Dunlop, M. Yoshita, et al., "Solar Cell Efficiency Tables (Version 64)," *Progress in Photovoltaics: Research and Applications* 32 (2024): 425–441.

2. M. A. Green, E. D. Dunlop, G. Siefer, M. Yoshita, N. Kopidakis, and X. J. Hao, "Solar Cell Efficiency Tables (Version 61)," *Progress in Photovoltaics: Research and Applications* 31 (2022): 3–16.

3. M. A. Green, E. D. Dunlop, J. Hohl-Ebinger, et al., "Solar Cell Efficiency Tables (Version 60)," *Progress in Photovoltaics: Research and Applications* 30 (2022): 687–701.

4. https://www.longi.com/en/news/.

5. M. M. Moslehi, P. Kapur, J. Kramer, et al., "World-Record 20.6% Efficiency 156 mm x 156 mm Full-Square Solar Cells Using low-Cost Kerfless Ultrathin Epitaxial Silicon & Porous Silicon Lift-Off Technology for Industry-Leading High-Performance Smart PV Modules," in *PV Asia Pacific Conference (APVIA/PVAP)*, 24 October 2012.

6. M. J. Keevers, T. L. Young, U. Schubert, and M. A. Green, "10% Efficient CSG Minimodules," in *22nd European Photovoltaic Solar Energy Conference*, Milan, September 2007 (Munich: WIP, 2008).

7. B. M. Kayes, H. Nie, R. Twist, et al., "27.6% Conversion Efficiency, a New Record for Single-Junction Solar Cells Under 1 Sun Illumination," in *Proceedings of the 37th IEEE Photovoltaic Specialists Conference* (Piscataway: IEEE, 2011).

8. R. Venkatasubramanian, B. C. O'Quinn, J. S. Hills, et al., "18.2% (AM1.5) Efficient GaAs Solar Cell on Optical-Grade Polycrystalline Ge Substrate," in *Conference Record, 25th IEEE Photovoltaic Specialists Conference, Washington, May 1997*, 31–36 (Piscataway: IEEE, 1997).

9. Wanlass M. *Systems and Methods for Advanced Ultra-High-Performance InP Solar Cells*. US Patent 9,590,131 B2, 7 March 2017 (Washington: US Patent and Trademark Office, 2017).

10. M. Nakamura, K. Yamaguchi, Y. Kimoto, Y. Yasaki, T. Kato, and H. Sugimoto, "Cd-Free Cu (In,Ga)(Se,S)2 Thin-Film Solar Cell With a new World Record Efficacy of 23.35%," in *46th IEEE PVSC, Chicago, IL, June 19* (Piscataway: IEEE, 2019) (see also http://www.solar-frontier.com/eng/news/2019/0117_press.html).

11. R. Diermann, *Avancis Claims 19.64% Efficiency for CIGS Module* (PV Magazine International, March 4, 2021) (https://www.pv-magazine.com/2021/03/04/avancis-claims-19-64-efficiency-for-cigs-module/).

12. *First Solar Press Release, First Solar Builds the Highest Efficiency Thin Film PV Cell on Record*, 5 August 2014.

13. J. Zhou, X. Xu, H. Wu, et al., "Control of the Phase Evolution of Kesterite by Tuning of the Selenium Partial Pressure for Solar Cells With 13.8% Certified Efficiency," *Nature Energy* 8 (2023): 526–535.

14. C. Yan, J. Huang, K. Sun, et al., "$Cu_2ZnSn\ S_4$ Solar Cells With Over 10% Power Conversion Efficiency Enabled by Heterojunction Heat Treatment," *Nature Energy* 3 (2018): 764–772.

15. T. Matsui, A. Bidiville, H. Sai, et al., "High-Efficiency Amorphous Silicon Solar Cells: Impact of Deposition Rate on Metastability," *Applied Physics Letters* 106 (2015): 053901, https://doi.org/10.1063/1.4907001.

16. H. Sai, T. Matsui, H. Kumagai, and K. Matsubara, "Thin-Film Microcrystalline Silicon Solar Cells: 11.9% Efficiency and Beyond," *Applied Physics Express* 11 (2018): 022301.

17. https://www.chemborun.com/news/latest-record-of-perovskite-solar-cells.html.

18. https://www.electronicsonline.net.au/content/power/news/nus-scientists-record-24-35-pce-for-perovskite-solar-cells-482262938.

19. https://www.perovskite-info.com/krict-and-unitest-develop-large-area-perovskite-solar-cell-206-efficiency.

20. L. Han, A. Fukui, Y. Chiba, et al., "Integrated Dye-Sensitized Solar Cell Module With Conversion Efficiency of 8.2%," *Applied Physics Letters* 94 (2009): 013305, https://doi.org/10.1063/1.3054160.

21. R. Komiya, A. Fukui, N. Murofushi, N. Koide, R. Yamanaka, and H. Katayama, "Improvement of the Conversion Efficiency of a Monolithic Type Dye-Sensitized Solar Cell Module," in *Technical Digest, 21st International Photovoltaic Science and Engineering Conference*, Fukuoka, November 2011, 2C-5O-08.

22. J. Faisst, E. Jiang, S. Bogati, et al., "Organic Solar Cell with an Active Area > 1 cm^2 Achieving 15.8% Certified Efficiency Using Optimized VIS-NIR Anti-Reflection Coating," *Solar RRL* 7 (2023): 2300663.

23. https://www.pv-magazine.com/2021/03/17/organic-pv-module-with-12-36-efficiency/.

24. R. Basu, F. Gumpert, J. Lohbreier, et al., "Large-Area Organic Photovoltaic Modules With 14.5% Certified World Record Efficiency," *Joule* 8 (2024): 970–978.

25. C. C. Boyd, R. Cheacharoen, T. Leijtens, and M. D. McGehee, "Understanding Degradation Mechanisms and Improving Stability of Perovskite Photovoltaics," *Chemical Reviews* 119 (2019): 3418–3451.

26. Y. Yang and J. You, "Make perovskite solar cells stable," *Nature* 544 (2017): 155–156.

27. U. O. Krašovec, M. Bokalič, and M. Topič, "Ageing of DSSC Studied by Electroluminescence and Transmission Imaging," *Solar Energy Materials and Solar Cells* 117 (2013): 67–72.

28. D. M. Tanenbaum, M. Hermenau, E. Voroshazi, et al., "The ISOS-3 Inter-Laboratory Collaboration Focused on the Stability of a Variety of Organic Photovoltaic Devices," *RSC Advances* 2 (2012): 882–893.

29. F. C. Krebs, ed., *Stability and Degradation of Organic and Polymer Solar Cells* (*Wiley, Chichester*, 2012). K. Norrman, S. A. Gevorgyan, T. Tromholt, B. Andreasen, and F. C. Krebs, "Stability of Polymer Solar Cells," *Advanced Materials* 24 (2012): 580–612.

30. M. A. Green, "The Passivated Emitter and Rear Cell (PERC): From Conception to Mass Production," *Solar Energy Materials and Solar Cells* 143 (2015): 190–197.

31. A. Richter, J. Benick, F. Feldmann, A. Fell, M. Hermle, and S. W. Glunz, "N-Type Si Solar Cells With Passivating Electron Contact: Identifying Sources for Efficiency Limitations by Wafer Thickness and Resistivity Variation," *Solar Energy Materials and Solar Cells* 173 (2017): 96–105.

32. F. Haase, C. Klamt, S. Schäfer, et al., "Laser Contact Openings for Local Poly-Si-Metal Contacts Enabling 26.1%-Efficient POLO-IBC Solar Cells," *Solar Energy Materials and Solar Cells* 186 (2018): 184–193.

33. Q. Wang, "Status of Crystalline Silicon PERC Solar Cells," in *NIST/UL Workshop on Photovoltaic Materials Durability*, Gaithersburg, MD USA, Dec 12-13, 2019.

34. https://static.trinasolar.com/eu-en/resources/newsroom/eu-trina solar-sets-27th-world-record-n-type-i-topcon-cell-achieving-259.

35. H. Lin, M. Yang, X. Ru, et al., "Silicon Heterojunction Solar Cells With Up to 26.81% Efficiency Achieved by Electrically Optimized Nanocrystalline-Silicon Hole Contact Layers," *Nature Energy* 8 (2023): 789–799.

36. *LONGi Achieves New World Record for p-Type Solar Cell Efficiency*. Press Release: 20 September 2022, https://www.longi.com/en/news/p-type-hjt-record/.

37. *NREL, Private Communication*, 22 May 2019.

38. K. Keller, K. Kiselman, O. Donzel-Gargand, et al., "High-Concentration Silver Alloying and Steep Back-Contact Gallium Grading Enabling Copper Indium Gallium Selenide Solar Cell With 23.6% Efficiency," *Nature Energy* 9 (2024): 467–478.

39. *First Solar Press Release*. First Solar Achieves yet Another Cell Conversion Efficiency World Record, 24 February 2016.

40. X. Cui, K. Sun, J. Huang, et al., "Cd-Free Cu2ZnSnS4 Solar Cell With an Efficiency Greater Than 10% Enabled by Al2O3 Passivation Layer," *Energy & Environmental Science* 12 (2019): 2751–2764.

41. http://en.ustc.edu.cn/info/1007/4676.htm.

42. L. Zhu, Z. Ming, J. Xu, et al., "Single-Junction Organic Solar Cells With Over 19% Efficiency Enabled by a Refined Double-Fibril Network Morphology," *Nature Materials* 21 (2022): 1–8, https://doi.org/10.1038/s41563-022-01244-y.

43. Y. Ren, D. Zhang, J. Suo, et al., "Hydroxamic Acid Pre-Adsorption Raises the Efficiency of Cosensitized Solar Cells," *Nature* 613, no. 7942 (2023): 60–65.

44. Sasaki K, Agui T, Nakaido K, Takahashi N, Onitsuka R, Takamoto T. *Proceedings, 9th International Conference on Concentrating Photovoltaics Systems, Miyazaki, Japan* 2013.

45. P. Schygulla, R. Müller, O. Höhn, et al., "Wafer-Bonded Two-Terminal III-V//Si Triple-Junction Solar Cell With Power Conversion Efficiency of 36.1% at AM1.5g," in *Presented at the 40th EU PVSEC, Lisbon* (Munich: WIP, 2023) Paper 2DO.9 (submitted to *Prog.Photovolt. Res. Appl.).*

46. S. Essig, C. Allebé, T. Remo, et al., "Raising the One-Sun Conversion Efficiency of III–V/Si Solar Cells to 32.8% for Two Junctions and 35.9% for Three Junctions," *Nature Energy* 2 (2017): 17144, https://doi.org/10.1038/nenergy.2017.144.

47. M. Feifel, D. Lackner, J. Schön, et al., "Epitaxial GaInP/GaAs/Si Triple-Junction Solar Cell With 25.9% AM1.5g Efficiency Enabled by Transparent Metamorphic $Al_xGa_{1-x}As_yP_{1-y}$ Step-Graded Buffer Structures," *Solar RRL* 5 (2021): 2000763, https://doi.org/10.1002/solr.202000763.

48. T. J. Grassman, D. J. Chmielewski, S. D. Carnevale, J. A. Carlin, and S. A. Ringel, "$GaAs_{0.75}P_{0.25}$/Si Dual-Junction Solar Cells Grown by MBE and MOCVD," *IEEE Journal of Photovoltaics* 6 (2016): 326–331.

49. M. A. Green, M. J. Keevers, B. Concha Ramon, et al., "Improvements in Sunlight to Electricity Conversion Efficiency: Above 40% for Direct Sunlight and Over 30% for Global," in *Paper 1AP.1.2,* European Photovoltaic Solar Energy Conference 2015, Hamburg, September 2015 (Munich: WIP, 2015).

50. https://www.longi.com/en/feature-report/world-record-for-solar-cell-efficiency/.

51. M. Jošt, E. Köhnen, A. Al-Ashouri, et al., "Perovskite/CIGS Tandem Solar Cells: From Certified 24.2% Toward 30% and Beyond," *ACS Energy Letters* 7 (2022): 1298–1307.

52. R. Lin, J. Xu, M. Y. Wei, et al., "All-Perovskite Tandem Solar Cells With Improved Grain Surface Passivation," *Nature* 603 (2022): 73–78.

53. H. Gao, K. Xiao, R. Lin, et al., "Homogeneous Crystallization and Buried Interface Passivation for Perovskite Tandem Solar Modules," *Science* 383 (2024): 855–859, https://doi.org/10.1126/science.adj6088.

54. H. Sai, T. Matsui, T. Koida, and K. Matsubara, "Stabilized 14.0%-Efficient Triple-Junction Thin-Film Silicon Solar Cell," *Applied Physics Letters* 109 (2016): 183506, https://doi.org/10.1063/1.49669996.

55. T. Matsui, K. Maejima, A. Bidiville, et al., "High-Efficiency Thin-Film Silicon Solar Cells Realized by Integrating Stable a-Si:H Absorbers Into Improved Device Design," *Japanese Journal of Applied Physics* 54 (2015): 08KB10, https://doi.org/10.7567/JJAP.54.08KB10.

56. http://mldevices.com/index.php/news/ (accessed 28 October 2018).

57. J. F. Geisz, M. A. Steiner, N. Jain, et al., "Building a Six-Junction Inverted Metamorphic Concentrator Solar Cell," *IEEE Journal of Photovoltaics* 8 (2018): 626–632.

58. K. Makita, Y. Kamikawa, H. Mizuno, et al., "III-V//$Cu_xIn_{1-y}Ga_ySe_2$ Multijunction Solar Cells With 27.2% Efficiency Fabricated Using Modified Smart Stack Technology With Pd Nanoparticle Array and Adhesive Material," *Progress in Photovoltaics: Research and Applications* 29 (2021): 887–898, https://doi.org/10.1002/pip.3398.

59. X. Wang, D. Zhang, B. Liu, et al., "Highly Efficient Perovskite/Organic Tandem Solar Cells Enabled by Mixed-Cation Surface Modulation," *Advanced Materials* 35 (2023): 2305946, https://doi.org/10.1002/adma.202305946.

60. L. S. Mattos, S. R. Scully, M. Syfu, et al., "New Module Efficiency Record: 23.5% Under 1-Sun Illumination Using Thin-Film Single-Junction GaAs Solar Cells," in *Proceedings of the 38th IEEE Photovoltaic Specialists Conference* (Munich: WIP, 2012).

61. H. Sugimoto, "High Efficiency and Large Volume Production of CIS-Based Modules," in *40th IEEE Photovoltaic Specialists Conference*, Denver, June 2014 (Piscataway: IEEE, 2014).

62. http://www.firstsolar.com/en-AU/-/media/First-Solar/Technical-Documents/Series-6-Datasheets/Series-6-Datasheet.ashx (accessed 28 October 2019).

63. https://taiyangnews.info/solaeon-technology-announces-world-record-for-perovskite-modules/.

64. M. Hosoya, H. Oooka, H. Nakao, et al., "Organic Thin Film Photovoltaic Modules," in *Proceedings of the 93rd Annual Meeting of the Chemical Society of Japan* (2013): 21–37.

65. *Sharp Achieves World's Highest Conversion Efficiency of 32.65% in a Lightweight, Flexible, Practically Sized Solar Module*. Press Release: June 6, 2022, https://global.sharp/corporate/news/220606-a.html.

66. https://www.oxfordpv.com/news/oxford-pv-debuts-residential-solar-module-record-setting-269-efficiency.

67. J. S. Cashmore, M. Apolloni, A. Braga, et al., "Improved Conversion Efficiencies of Thin-Film Silicon Tandem (MICROMORPH ™) Photovoltaic Modules," *Solar Energy Materials and Solar Cells* 144 (2016): 84–95, https://doi.org/10.1016/j.solmat.2015.08.022.

68. V. Bheemreddy, L. BJJ, A. Wills, and C. P. Murcia, "Life Prediction Model Development for Flexible Photovoltaic Modules Using

Accelerated Damp Heat Testing," in *IEEE 7th World Conf. on Photovoltaic Energy Conversion (WCPEC)* (2018): 1249–1251.

69. T. Takamoto, H. Juso, K. Ueda, et al., "IMM Triple-Junction Solar Cells and Modules Optimized for Space and Terrestrial Conditions," in *Proceedings of the 44th IEEE Photovoltaic Specialist Conference (PVSC)* (Piscataway, IEEE, 2017), https://doi.org/10.1109/PVSC.2017.8366097.

70. www.renshinesolar.com.

71. A. Slade and V. Garboushian, "27.6% Efficient Silicon Concentrator Cell for Mass Production," in *Technical Digest, 15th International Photovoltaic Science and Engineering Conference*, Shanghai, October 2005, 701.

72. J. S. Ward, K. Ramanathan, F. S. Hasoon, et al., "A 21.5% Efficient Cu (In,Ga)Se2 Thin-Film Concentrator Solar Cell," *Progress in Photovoltaics: Research and Applications* 10 (2002): 41–46.

73. F. Dimroth, T. N. D. Tibbits, M. Niemeyer, et al., "Four-Junction Wafer-Bonded Concentrator Solar Cells," *IEEE Journal of Photovoltaics* 6, no. 1 (2016): 343–349, https://doi.org/10.1109/JPHOTOV.2015.2501729.

74. *NREL Press Release NR-4514*, 16 December 2014.

75. *Press Release, Sharp Corporation*, 31 May 2012 (accessed at http://sharp-world.com/corporate/news/120531.html on 5 June 2013).

76. N. Jain, K. L. Schulte, J. F. Geisz, et al., "High-Efficiency Inverted Metamorphic 1.7/1.1 eV GaInAsP/GaInAs Dual-Junction Solar Cells," *Applied Physics Letters* 112 (2018): 053905.

77. M. Steiner, G. Siefer, T. Schmidt, M. Wiesenfarth, F. Dimroth, and A. W. Bett, "43% Sunlight to Electricity Conversion Efficiency Using CPV," *IEEE Journal of Photovoltaics* 6, no. 4 (2016): 1020–1024, https://doi.org/10.1109/JPHOTOV.2016.2551460.

78. M. A. Green, M. J. Keevers, I. Thomas, J. B. Lasich, K. Emery, and R. R. King, "40% Efficient Sunlight to Electricity Conversion," *Progress in Photovoltaics: Research and Applications* 23, no. 6 (2015): 685–691.

79. C. J. Chiang and E. H. Richards, "A 20% Efficient Photovoltaic Concentrator Module," in *Conf. Record, 21st IEEE Photovoltaic Specialists Conference*, Kissimimee, May 1990, 861–863 (Piscataway: IEEE, 1990).

80. http://amonix.com/pressreleases/amonix-achieves-world-record-359-module-efficiency-rating-nrel-4 (accessed 23 October 2013).

81. S. van Riesen, M. Neubauer, A. Boos, et al., "New Module Design With 4-Junction Solar Cells for High Efficiencies," in *Proceedings of the 11th Conference on Concentrator Photovoltaic Systems* (2015).

82. J. F. Martínez, M. Steiner, M. Wiesenfarth, G. Siefer, S. W. Glunz, and F. Dimroth, "Power Rating Procedure of Hybrid CPV/PV Bifacial Modules," *Progress in Photovoltaics: Research and Applications* 29 (2021): 614–629.

83. F. Zhang, S. R. Wenham, and M. A. Green, "Large Area, Concentrator Buried Contact Solar Cells," *IEEE Transactions on Electron Devices* 42 (1995): 144–149.

84. L. H. Slooff, E. E. Bende, A. R. Burgers, et al., "A Luminescent Solar Concentrator With 7.1% Power Conversion Efficiency," *Physica Status Solidi (RRL)* 2, no. 6 (2008): 257–259.

85. M. Steiner, M. Wiesenfarth, J. F. Martínez, G. Siefer, and F. Dimroth, "Pushing Energy Yield With Concentrating Photovoltaics," in *AIP Conference Proceedings 2149, 060006* (Melville: AIP Publishing, 2019), https://doi.org/10.1063/1.5124199.

86. H. Müllejans, S. Winter, M. A. Green, and E. D. Dunlop, "What Is the Correct Efficiency for Terrestrial Concentrator PV Devices?" in *38th European Photovoltaic Solar Energy Conference*, Sept. 2021 (Munich: WIP, 2021).

87. C. A. Gueymard, D. Myers, and K. Emery, "Proposed Reference Irradiance Spectra for Solar Energy Systems Testing," *Solar Energy* 73 (2002): 443–467.

88. Program Milestones and Decision Points for Single Junction Thin Films," in *Annual Progress Report 1984, Photovoltaics, Solar Energy Research Institute*, Report DOE/CE-0128, vol. 7 (Golden CO: SERI, 1985).

89. I. Sakata, Y. Tanaka, and K. Koizawa, "Japan's New National R&D Program for Photovoltaics," in *Photovoltaic Energy Conversion, Conference Record of the 2006 IEEE 4th World Conference*, vol. 1 (Piscatawy NJ: IEEE, 2008): 1–4.

90. Jäger-Waldau, A (Ed.). *PVNET:* European Roadmap for PV R&D, *EUR 21087 EN*, 2004.